Chemocatalytic Amplification Probes Enable Transcriptionally-Regulated Au(I)-Catalysis in *E. coli* and Sensitive Detection of SARS-CoV-2 RNA Fragments

Sydnee A. Green, Benjamin Wigman, Sepand K. Nistanaki, Hayden R. Montgomery, Christopher G. Jones, Hosea M. Nelson*

Department of Chemistry and Biochemistry, University of California, Los Angeles, Los Angeles, CA, 90095, USA

*Corresponding Author Email: hosea@chem.ucla.edu (H.M.N.)

Abstract:

The union of transition metal catalysis with native biochemistry presents a powerful opportunity to perform abiotic reactions within complex biological systems (*1*,*2*). However, several chemical compatibility challenges associated with incorporating reactive metal centers into complex biological environments have hindered efforts in this area, despite the many opportunities it may present. More challenging than chemical compatibility is biocommunicative transition metal catalysis, where the reactivity of the metal species is regulated by native biological stimuli, akin to natural biocatalytic processes. Here we report a novel Au(I)-DNAzyme that is activated by short nucleic acids in a highly sequence-specific manner and that is compatible with complex biological matrices. The active Au(I)-DNAzyme catalyzes the formation of a fluorescent molecule with >10 turnovers. This functional allostery, resulting in chemocatalytic signal amplification, is competent in complex biological settings, including within recombinant *E. coli* cells, where the catalytic activity of the Au(I)-DNAzyme is regulated by transcription of an inducible plasmid. We further demonstrate the potential of this transition metal oligonucleotide complex as a highly sensitive and selective hybridization probe, permitting the detection of attomolar concentrations (*ca.* 60 molecules/μL) of SARS-CoV-2 RNA gene fragments in simulated biological matrices with ≥85%

accuracy. Notably, this sensitive detection platform avoids expensive and poorly-scalable biochemical components (e.g. post-synthetically modified oligonucleotides or enzymes) and instead utilizes small molecule fluorophores, inexpensive Au salts and oligonucleotides composed of canonical bases. This discovery highlights promising opportunities to perform abiotic catalysis in complex biological settings under transcriptional regulation, as well as a chemocatalytic strategy for PCR-free, direct-detection of RNA and DNA.

Introduction:

While transition metal catalysis has become a powerful and efficient tool in synthetic chemistry, its application in biology has trailed behind, as synthetic transition metal complexes struggle to avoid deleterious reactions with the diverse chemical functionalities present in biological media. The biocatalytic community has made great strides toward overcoming this challenge, demonstrating that engineering of wild-type metalloenzymes can lead to biocatalysts that mediate abiotic chemical transformations such as insertion and other metal-carbenoid reactions (*2*). In fewer examples, novel metalloenzymes with non-native metal centers have been reported, in some cases capable of mediating transformations well beyond the scope of wild-type biochemical transformations (*3–6*). Organometallic complexes have also found use in biological settings, although rarely employed catalytically *(8–10*).

Our group has become interested in developing transition metal catalysts that are not only functional under the challenge of biological conditions, but also regulated by gene transcription. In this scenario, we envisioned genotype-specific catalysis, where bioconjugation reactions and activation of pro-drugs or reporter molecules could be controlled temporally and spatially through transcriptional upregulation. Moreover, akin to biochemical amplification regimes such as polymerase chain reaction (PCR), we envisioned that signal amplification could be achieved

through this chemical catalysis, allowing for detection of infinitesimally-small quantities of gene transcripts for applications in chemical biology, genetics, and diagnostics. To this end, we previously reported an example of a novel Au(I)-DNAzyme that performs abiotic hydroamination reactions under highly sequence specific upregulation by short RNA or DNA fragments (**Figure 1**) (*11*). In the initial study, we provided proof-of-principle, but were not able to demonstrate efficacy in biological matrices as our Au(I)-DNAzyme proved to be poorly compatible with biological media. Herein we report the development of a new Au(I)-DNAzyme scaffold featuring a novel metal-binding motif comprised of a Au(I)-mediated cytosine–cytosine (C–C) base pair

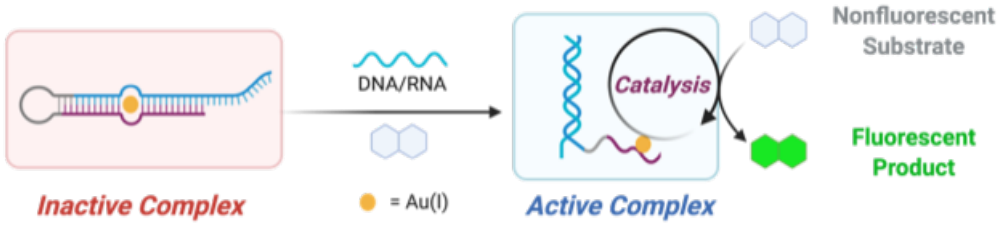

Figure 1. Activation of Au(I)-CAP with complementary DNA or RNA transcript.

with unprecedented thermal and biological stability. We show that this new Au(I)-DNAzyme is capable of catalyzing Friedel-Crafts-like reactions of alkynes in response to gene transcription in cellular extracts and inside living *E. coli* cells. We further demonstrate the application of this strategy to diagnostics, as we are able to directly detect attomolar (*ca*. 60 molecules/μL) quantities of RNA (≥85% accuracy). This is highlighted by the PCR-free, direct detection of SARS-CoV-2 RNA fragments in simulated saliva samples using our chemocatalytic amplification probes (CAPs).

Results and Discussion:

In previous studies we found that a Au(I) DNA complex could be formed through the incorporation of Au(I) into a DNA duplex containing a C–T mismatch, thereby increasing the thermal stability

of the duplex by 7 °C (*11*). At the outset of this current study, we hypothesized that other pyrimidine mismatches might also bind Au(I) ions in a similar fashion. Through thermal stability studies we ultimately discovered that DNA duplexes containing a C–C mismatch were significantly stabilized upon the addition of a Au(I) precursor (Me_2SAuCl), suggesting the formation of a stabilizing C–Au–C metal-mediated base pair (MMBP). Interestingly, treating DNA duplex **CC1** with two equivalents of Au(I) resulted in a large increase in thermal stability (ΔT_m = 33 °C), which was significant compared to the addition of only one equivalent of Au(I) (**Figure 2**). The addition of greater than two equivalents of Au(I) had minimal effect, and the corresponding "matched" C–G (**CG1**) or A–T (**AT1**) DNA sequences were also essentially unaffected by the addition of Au(I). These experiments suggest the selective incorporation of two Au(I) ions into a

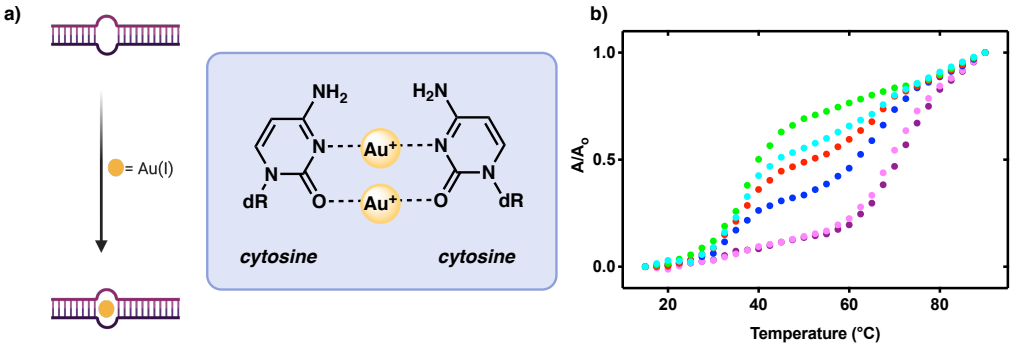

c)

entry	duplex		T_m (°C) with n equiv of $(Me_2S)AuCl$ n = 0	n = 1	n = 2	ΔT_m (°C)
1	5'-d(CCT TTC TCT CCC TC) 3'-d(GGA AAG AGA GGG AG)	CG1	55.6 ± 0.3	60.0 ± 0.5	—	4.4 ± 0.6[a]
2	5'-d(CCT TTC TAT CCC TC) 3'-d(GGA AAG ATA GGG AG)	AT1	52.4 ± 0.3	53.8 ± 0.3	—	1.4 ± 0.4
3	5'-d(CCT TTC TCT CCC TC) 3'-d(GGA AAG ACA GGG AG)	CC1	38.3 ± 0.9	35.2 ± 0.8 67.1 ± 1.4[b]	71 ± 1	33 ± 3

Figure 2. a) Thermal denaturation curves for CC1 duplex with varying equivalents of Au(I) (0, 0.4, 1.0, 1.4, 2.0, 3.0) (• 0 equiv. $(Me_2S)AuCl$, • 0.4 equiv. $(Me_2S)AuCl$, • 1.0 equiv. $(Me_2S)AuCl$, • 1.4 equiv. $(Me_2S)AuCl$, • 2.0 equiv. $(Me_2S)AuCl$, • 3.0 equiv. $(Me_2S)AuCl$). b) Addition of $(Me_2S)AuCl$ to DNA mismatch and incorporation of Au(I) ion c) T_m values for matches and pyrimidine mismatches. [a]Increase in CG1 due to known favorable interactions between gold, cytosine, and guanine. [b]Two values reported due to biphasic melting.

C–C mismatch. We propose that two Au(I) ions bind between the endocyclic nitrogens and carbonyl oxygens of the cytosine–cytosine mismatch, based on previous reported structures of Ag(I) MMBPs (**Figure 2a**) (*12*,*13*). This dramatic increase in thermal stability is notable as similar increases have only been observed when synthetic bases are employed or when a covalent cross link has been introduced between the nucleic acid strands (*14–16*).

Encouraged by the strong binding of Au(I) to C–C mismatches, which implied a potential for greater stability in complex chemical environments, we attempted to incorporate Au(I) into a hairpin sequence to forge a Au(I)-DNAzyme. We envisioned that two Au(I) ions could be incorporated into a hairpin sequence containing a single C–C mismatch, providing a coordinatively saturated metal complex. Addition of a complementary nucleic acid strand induces strand displacement revealing a coordination site on the metal (**Figure 3a**). Presumably, binding of alkyne **1** to this coordination site initiates cyclization to a fluorescent coumarin product **2 (Figure 3b)** (*17*). In initial experiments, we were pleased to find that activation of a 250 nM solution of the Au(I)-DNA complex with one catalytic equivalent of complement initiated nearly 13 catalytic turnovers based on the concentration of Au(I) added. Importantly, without addition of the complementary nucleic acid strand, there was approximately 0.1 turnovers (**Figure 3c**). This finding, though representing modest turnover numbers (TON) from a chemistry perspective, revealed the opportunity to achieve superior sensitivity to our previously reported system due to a dramatic decrease in background reactivity of the probe in the absence of a transcriptional activator (increased signal-to-noise ratio).

With the heightened sensitivity of this probe compared to our previously reported system (250 nM detection *vs.* 10 μM detection), we were compelled to compare the sensitivity of our CAP complexes to molecular beacons routinely used for sensing nucleic acids. Molecular beacons are

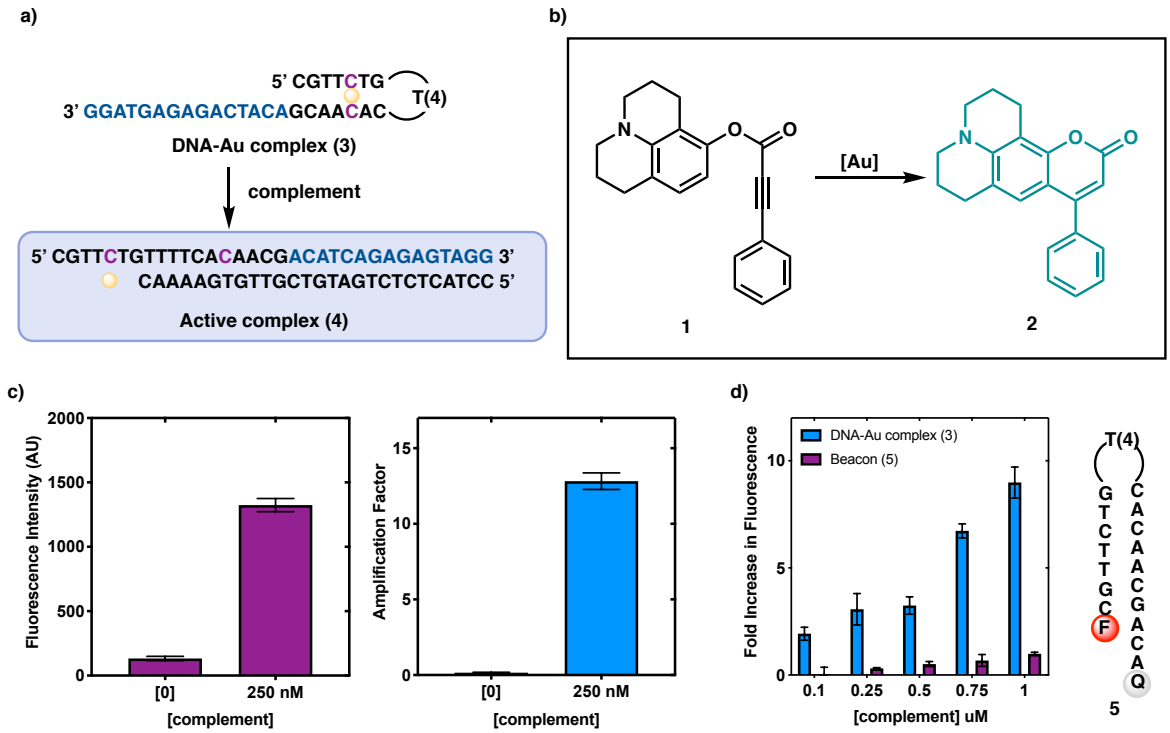

Figure 3. a) Inactive complex **3** hybridizes to complement to form active complex **4**. b) Profluorophore **1** cyclizes in presence of gold ions to form fluorescent coumarin product 2. c) Fluorescence intensity and amplification factor of complex **3** with profluorophore **1**. Amplification factor = [fluorescent product]/[complement]. d) Fold increase of DNA-Au complex **3** compared to molecular beacon **5** with varying concentrations of complement F = FAM, Q = DABCYL.

often used in conjunction with PCR for quantitative detection of nucleic acids (*18*,*19*). These FRET-based probes provide a single fluorescent output for every complementary nucleic acid that is hybridized, hence there is a need for amplification through PCR or other means to increase the amount of detectable nucleic acid present to meet the beacon's limit of detection (250 nM in our hands) (*20*). We hypothesized that our catalytic platform could overcome this inherent limitation given its ability to amplify signal through the catalytic production of >10 equivalents of fluorophore in response to a single hybridization event. Ultimately, this would allow entry to a more sensitive gene detection platform with improved limits of detection. Indeed, in direct comparison at 1 μM, addition of one equivalent of complementary sequence led to a 13-fold increase (fold increase = [fluorescence with complement]/[fluorescence with no complement]) in fluorescence with the Au(I)-CAP, compared to less than a 2-fold increase with the FRET-based

molecular beacon. At complement concentrations lower than one equivalent respective to probe, our Au(I)-CAP maintained over a 4-fold increase in fluorescence, whereas the detection limit of the molecular beacon was ~0.25 μM, above which there was only a 1.3-fold increase in fluorescence (**Figure 3d**).

The increased sensitivity of our CAP system inspired us to explore its ability to detect mRNA directly produced through transcription. The direct (PCR-free) detection of mRNA or DNA in cell lysates could contribute to several areas, including diagnostics and forensics, by lowering detection limits. We initially attempted to detect mRNA extracted from recombinant *E. coli* cells. We transformed competent *E. coli* cells with a plasmid containing our complement gene (gene X) and a T7 *lac* promoter. As an appropriate control, we transformed a group of cells with the plasmid that did not contain gene X (*21*). The cell lysate of both cell lines were incubated with our CAP at 1 μM and profluorophore **1** at 200 μM for 12 hours and subjected to confocal microscopy to visualize fluorescence. We observed that the cell lysate of the cells expressing the complement exhibited nearly a 3-fold increase in fluorescence when compared to the control cell lysate (**Figure 4a**).

To further assess the ability of our catalyst to perform in biologically relevant conditions, we incorporated the HP-Au(I) complex directly into competent *E. coli* cells using heat shock (**Figure 4b**) (*22*). After a three-hour incubation of *E. coli* transformed with gene X plasmids with 1 μM of the HP-Au(I) complex, followed by stringent washing, and a subsequent overnight incubation with profluorophore **1**, we observed that the cells expressing the complementary sequence (**Figure 4c**) were more fluorescent than the cells containing the control plasmid (**Figure 4d**). These results further demonstrate the ability of this novel Au(I)-DNAzyme to catalyze abiotic chemical transformations *in cellulo* in response to gene transcription, highlighting the potential for

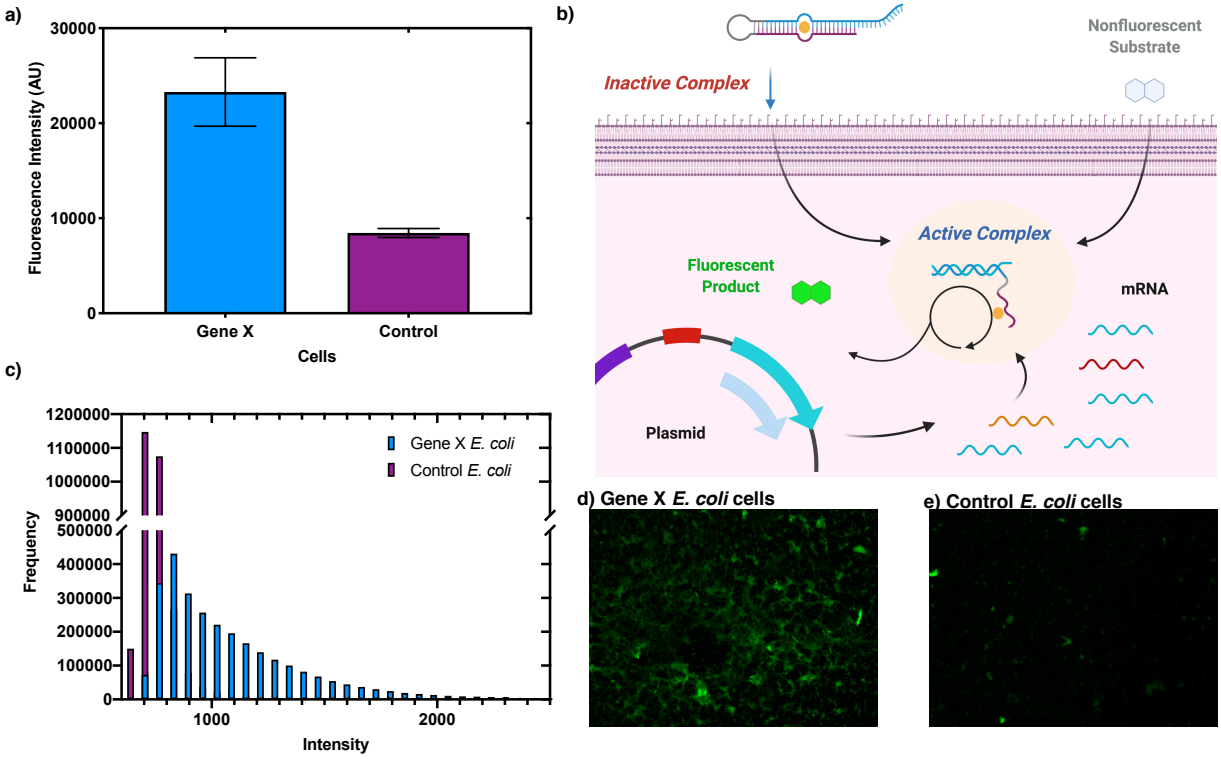

Figure 4. a) Fluorescence intensity in response to gene X and control cell lysates b) Au(I)-CAP incorporation into competent cells engineered to express the complementary sequence. c) Histogram of Frequency vs. Intensity of gene X and control E. coli cell fluorescene d) Fluorescence image of gene X engineered whole cells after incubation with Au(I)-CAP and profluorophore **1**. e) Fluorescence image of control whole cells after incubation with Au(I)-CAP and profluorophore **1**.

this technology to be used as a highly sensitive diagnostic tool for detection of nucleic acid material in both biotechnological and clinical applications.

Given the remarkable sensitivity of our Au(I)-CAP system for the detection of genetic information under biologically relevant conditions, we reasoned that the application of this technology to viral diagnostics could address an unmet biomedical need. In fact, while developing this system, we were met with the emergence of the COVID-19 pandemic, which highlighted the urgent need for improved diagnostic technologies. In particular, the current testing platform introduced by the Centers for Disease Control (CDC) relies on resource intensive reverse transcription/qPCR to amplify the viral RNA to meet the minimum detection limit of the FRET-based hybridization probe used in the COVID-19 test kit (*23*). The process requires cumbersome

procedures, sensitive reagents, and advanced molecular biology instrumentation, thereby limiting rapid deployment of low-cost tests on a large scale, with limited opportunity for point-of-care testing (*24*). Given these limitations, and the need for accurate, sensitive, and cost-efficient

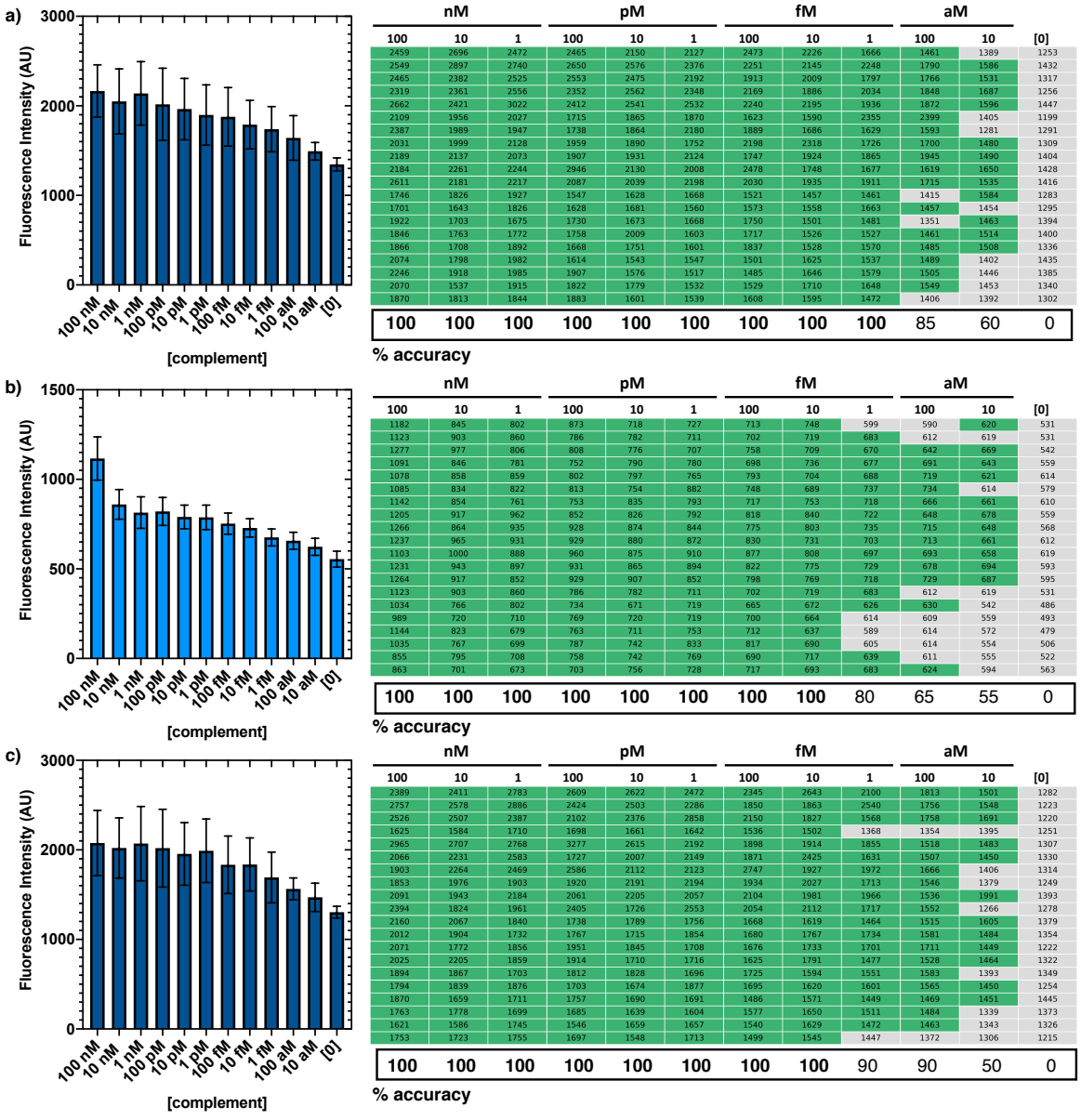

nM			pM			fM			aM		
100	10	1	100	10	1	100	10	1	100	10	[0]
2459	2696	2472	2465	2150	2127	2473	2226	1666	1461	1389	1253
2549	2897	2740	2650	2576	2376	2251	2145	2248	1790	1586	1432
2465	2382	2525	2553	2475	2192	1913	2009	1797	1766	1531	1317
2319	2361	2556	2352	2562	2348	2169	1886	2034	1848	1687	1256
2662	2421	3022	2412	2541	2532	2240	2195	1936	1872	1596	1447
2109	1956	2027	1715	1865	1870	1623	1590	2355	2399	1405	1199
2387	1989	1947	1738	1864	2180	1889	1686	1629	1593	1281	1291
2031	1999	2128	1959	1890	1752	2198	2318	1726	1700	1480	1309
2189	2137	2073	1907	1931	2124	1747	1924	1865	1945	1490	1404
2184	2261	2244	2946	2130	2008	2478	1748	1677	1619	1650	1428
2611	2181	2217	2087	2039	2198	2030	1935	1911	1715	1535	1416
1746	1826	1927	1547	1628	1668	1521	1457	1461	1415	1584	1283
1701	1643	1826	1628	1681	1560	1573	1558	1663	1457	1454	1295
1922	1703	1675	1730	1673	1668	1750	1501	1481	1351	1463	1394
1846	1763	1772	1758	2009	1603	1717	1526	1527	1461	1514	1400
1866	1708	1892	1668	1751	1601	1837	1528	1570	1485	1508	1336
2074	1798	1982	1614	1543	1547	1501	1625	1537	1489	1402	1435
2246	1918	1985	1907	1576	1517	1485	1646	1579	1505	1446	1385
2070	1537	1915	1822	1779	1532	1529	1710	1648	1549	1453	1340
1870	1813	1844	1883	1601	1539	1608	1595	1472	1406	1392	1302
100	100	100	100	100	100	100	100	100	85	60	0

% accuracy

nM			pM			fM			aM		
100	10	1	100	10	1	100	10	1	100	10	[0]
1182	845	802	873	718	727	713	748	599	590	620	531
1123	903	860	786	782	711	702	719	683	612	619	531
1277	977	806	808	776	707	758	709	670	642	669	542
1091	846	781	752	790	780	698	736	677	691	643	559
1078	858	859	802	797	765	793	704	688	719	621	614
1085	834	822	813	754	882	748	689	737	734	614	579
1142	854	761	753	835	793	717	753	718	666	661	610
1205	917	962	852	826	792	818	840	722	648	678	559
1266	864	935	928	874	844	775	803	735	715	648	568
1237	965	931	929	880	872	830	731	703	713	661	612
1103	1000	888	960	875	910	877	808	697	693	658	619
1231	943	897	931	865	894	822	775	729	678	694	593
1264	917	852	929	907	852	798	769	718	729	687	595
1123	903	860	786	782	711	702	719	683	612	619	531
1034	766	802	734	671	719	665	672	626	630	542	486
989	720	710	769	720	719	700	664	614	609	559	493
1144	823	679	763	711	753	712	637	589	614	572	479
1035	767	699	787	742	833	817	690	605	614	554	506
855	795	708	758	742	769	690	717	639	611	555	522
863	701	673	703	756	728	717	693	683	624	594	563
100	100	100	100	100	100	100	100	80	65	55	0

% accuracy

nM			pM			fM			aM		
100	10	1	100	10	1	100	10	1	100	10	[0]
2389	2411	2783	2609	2622	2472	2345	2643	2100	1813	1501	1282
2757	2578	2886	2424	2503	2286	1850	1863	2540	1756	1548	1223
2526	2507	2387	2102	2376	2858	2150	1827	1568	1758	1691	1220
1625	1584	1710	1698	1661	1642	1536	1502	1368	1354	1395	1251
2965	2707	2768	3277	2615	2192	1898	1914	1855	1518	1483	1307
2066	2231	2583	1727	2007	2149	1871	2425	1631	1507	1450	1330
1903	2264	2469	2586	2112	2123	2747	1927	1972	1666	1406	1314
1853	1976	1903	1920	2191	2194	1934	2027	1713	1546	1379	1249
2091	1943	2184	2061	2205	2057	2104	1981	1966	1536	1991	1393
2394	1824	1961	2405	1726	2553	2054	2112	1717	1552	1266	1278
2160	2067	1840	1738	1789	1756	1668	1619	1464	1515	1605	1379
2012	1904	1732	1767	1715	1854	1680	1767	1734	1581	1484	1354
2071	1772	1856	1951	1845	1708	1676	1733	1701	1711	1449	1222
2025	2205	1859	1914	1710	1716	1625	1791	1477	1528	1464	1322
1894	1867	1703	1812	1828	1696	1725	1594	1551	1583	1393	1349
1794	1839	1876	1703	1674	1877	1695	1620	1601	1565	1450	1254
1870	1659	1711	1757	1690	1691	1486	1571	1449	1469	1451	1445
1763	1778	1699	1685	1639	1604	1577	1650	1511	1484	1339	1373
1621	1586	1745	1546	1659	1657	1540	1629	1472	1463	1343	1326
1753	1723	1755	1697	1548	1713	1499	1545	1447	1372	1306	1215
100	100	100	100	100	100	100	100	90	90	50	0

% accuracy

Figure 5. a) Fluorescence intensity of **rHP6** with viral RNA fragment in 125 mM $NaClO_4$, 4% synthetic saliva, 10 µg/ml salmon testes DNA and LOD of reactions defined by using 1455 (2 standard deviations above no complement average) as threshold fluorescence after 8 hours. b) Fluorescence intensity of **dHP1** with viral DNA reverse transcript in 125 mM $NaClO_4$, 4% synthetic saliva, 10 µg/ml salmon testes DNA and LOD of reactions defined by using 620 as threshold fluorescence after 4 hours. c) Fluorescence intensity of **Hs_RPP30** with RNA transcript in 125 mM $NaClO_4$, 4% synthetic saliva, 10 µg/ml salmon testes DNA and LOD of reactions defined by using as threshold fluorescence after 8 hours.

COVID-19 diagnostics (*25*), we felt responsible to translate our newly developed catalytic system toward a COVID-19 diagnostics platform. The observed signal amplification and superior sensitivity of our system over standard molecular beacon platforms highlighted a strategic opportunity to contribute to the field during this unprecedented time.

In initial efforts, we designed several Au(I)-CAPs complementary to various portions of the SARS-CoV-2 genome (**see SI**). From an examination of hairpin structures that hybridize to the N gene of the viral genome, hairpin **rHP6** (5'-AGT CGC AGC ACA GCT CGC TGG TCC AGA ACT GAT TTT TCA CTT CTG G-3') resulted in a significant increase in fluorescence when exposed to 100 nM of the complementary RNA sequence with 95% accuracy, using a limit of detection (LOD) threshold analogous to FDA regulations (*26*). Further comparison of the mean intensities using one-way ANOVA and the Tukey-Kramer Honestly Significant Difference (HSD) test ($p < 0.0001$) however, show a significant difference in mean intensities down to 10 fM (**Figure SX.1**) when compared to conditions without the complementary sequence. Given these promising initial experiments, we were eager to see if the **rHP6** Au(I)-CAP would be compatible with conditions relevant to real human samples. Interestingly, conducting these experiments in a solution of synthetic saliva containing 10 ug/mL of random sequence DNA (salmon testes DNA) showed an increase in sensitivity, with >95% of the values above the threshold for 1 fM of complementary RNA fragment (**Figure 5a**). In addition, examination of Au(I)-CAPs complementary to other segments of viral transcript DNA revealed a sequence (**dHP1** 5'-GAG GGA GCC TTG AAT ACA CCA AAA GAT CAC ATT GGT TTT CCA ATC TGA TC-3') with an LOD of 10 fM (**Figure 5b**). These sequences outperform the current molecular beacon used in the current CDC test (2019-nCOV_N1 probe – FAM, BHQ-1) in the direct detection

complementary transcripts (250 nM in our hands without PCR amplification) by an astounding 10^7-fold increase in sensitivity.

Similar to previously reported COVID-19 detection assays, we designed a Au(I)-CAP complex to detect transcripts of the human RNAse P gene as a positive control for RNA extraction (*28*,*29*). We found that this Au(I)-CAP (**Hs_RPP30** 5'-CCG CGC AGA GCC TTC AGG TCA GAA TTT TTT CTC ACC T-3') has exceptional sensitivity and low background reactivity. Akin to our hairpin complex for the SARS-CoV-2 N gene (**rHP6**), we were able to detect femtomolar (10 fM, ≥95% accuracy) concentrations of the human RNAse P gene transcript after 2 hours (**Figure 5c**). Importantly, we found that the addition of short nucleic acid fragments that are non-complementary to **rHP6** or **Hs_RPP30** do not result in an increase in fluorescence; Only the addition of the complementary sequence leads to the formation of fluorescent product and therefore selective detection of short nucleic acids can be achieved through this system (29).

Kinetic experiments of **rHP6** revealed a significant increase in fluorescence of the solutions containing complement within the first several hours, Figure 6 shows the change in each concentration's probability distribution over time. After the first 60 minutes there is no overlap between 100 nM and the no complement reaction, meaning that all of the values at 100 nM have surpassed the LOD threshold after 60 minutes (**Figure 6a**). After only 180 minutes, the fluorescence values of

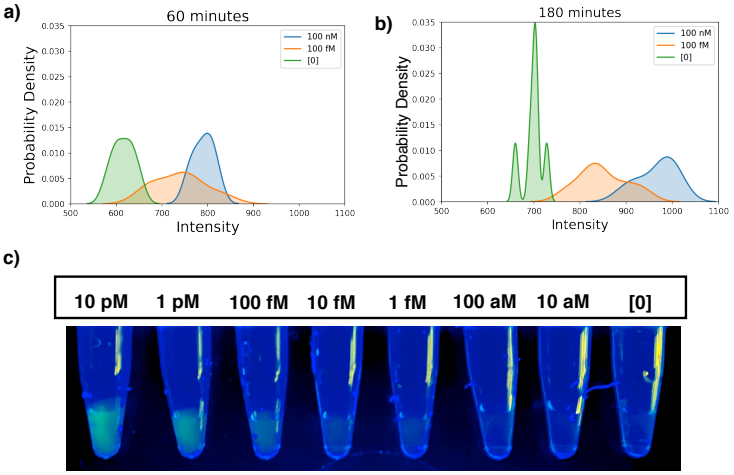

Figure 6. Probability distribution of mean intensities for rHP6 with 100 nM, 100 fM, and [0] of complement DNA at a) 60 minutes and b) 180 minutes. c) Fluorescence of reaction under long wave lamp (390 nm) after 36 hours.

the reactions containing 100 fM of complement have very little overlap with the no complement reactions and are near the LOD (**Figure 6b**). While at early time points, the fluorescence is fairly low, after 36 hours, the fluorescence differences are visible to the eye under long wave UV irradiation using an inexpensive hand held TLC lamp (**Figure 6c**). Longer reaction times resulted in an increase in the background from the experiment containing no complement. This background is likely due to leaching of gold and decomposition of the hairpin-Au complex.

Conclusion

In conclusion, we have discovered and developed a novel C–C MMBP, wherein the incorporation of two equivalents of Au(I) ions results in an unprecedented level of thermal stabilization (ΔT_m = 33 ºC). We have demonstrated that, despite the inherent stability of these Au-DNA complexes, they are able to effectively hybridize to low concentrations of complementary nucleic acid strands, and activate the catalytic activity of the Au(I) metal center. These findings permitted the detection of low concentrations of mRNA in complex biological matrices such as cell lysates and whole cells, and were competitively more sensitive than standard molecular beacon technologies. This system shows promise as an inexpensive and fast detection method for DNA and RNA. We have demonstrated one such application in the early development of a COVID detection method, which culminated in the ability to detect femtomolar to attomolar concentrations of viral RNA fragments with ≥85% accuracy. Often methods to detect genetic information require expensive enzymes, probes, or instrumentation, however, we have demonstrated the detection of femtomolar concentrations of short nucleic acid transcripts with simple coumarin probes and inexpensive gold salts that could ultimately lead to the development of a cheap and accessible point-of-care viral diagnostics test. We are currently optimizing this system to achieve direct detection of viral genetic information from clinical samples.

Materials and Methods:

CAP Enabled Detection of RNA/DNA sequences:

To each well of a black, opaque 100uL polypropylene 96 well plate was added $NaClO_4$/synthetic saliva solution (20uL, final concentration 165mM $NaClO_4$, 10 ug/mL exogenous salmon testes DNA). To these wells was added the desired concentration DNA/RNA fragment as an aqueous solution (10 uL). To each well was added a freshly prepared (~15 minutes incubation time) 0.015% acetone v/v aqueous solution of pre-complexed Me_2S•AuCl/35-mer oligonucleotide solution (20uL, final concentration 100nM). To each well was added an 80% ethanol v/v aqueous solution of the profluorophore (50uL, final concentration 200uM 40% ethanol v/v aqueous solution), 2,3,6,7-tetrahydro-1*H*,5*H*-pyrido[3,2,1-*ij*]quinolin-8-yl 3-phenylpropiolate, and the solution mixed by pipette (50uL 3 times). The plate was sealed with a clear adhesive cover and allowed to sit at room temperature for the desired time. The cover was removed and the plate was inserted into a Teacan M1000 plate reader. Fluorescence spectra were recorded for each well as an average of 9 readings (420nM Excitation, 535nM Emission, Gain=150, Z-height=24333).

Data Availability.

Further fluorescence measurements, NMR spectra, cell images, and thermal stability measurements can be found in the *SI Appendix.*

Acknowledgements.

Financial support for this work was generously provided by the David and Lucile Packard Foundation (to H.M.N.), the Pew Charitable Trusts (to H.M.N), Bristol Myers Squibb (to H.M.N.), the UCLA AIDS institute (to H.M.N.) and the National Science Foundation (DGE-1650604 to B.W. and C.G.J.). S.A.G. thanks the Department of Chemistry and Biochemistry

UCLA Fellowship for funding. B.W. thanks the Christopher S. Foote Fellowship for funding. S.K.N. thanks the USPHS National Research Service Award (T32GM008496). The authors thank the UCLA Molecular Instrumentation Center for NMR and mass spectrometry instrumentation. This material is based on work supported by the National Institutes of Health under instrumentation (1S10OD016387-01). We would like to thank Dr. Mark Arbing for assistance and the UCLA-DOE Protein Expression Core for *E. coli* cell transformation and expression. We would like to thank Amir Nasajpour for assistance with cell imaging. We would like to acknowledge Professor F. Dean Toste (UC Berkeley) for useful discussions.

Author Contributions.

H.M.N. conceived of project and designed experiments. S.A.G., B.W., S.K.N., and H.R.M. designed and conducted experiments. C.G.J. performed statistical analyses. H.M.N., S.A.G., B.W., S.K.N., and C.G.J. prepared the manuscript.

1. H.-T. Hsu, B. M. Trantow, R. M. Waymouth, P. A. Wender, Bioorthogonal Catalysis: A General Method To Evaluate Metal-Catalyzed Reactions in Real Time in Living Systems Using a Cellular Luciferase Reporter System. *Bioconjugate Chem.* **27**, 376-382 (2016).

2. K. Chen, F. H. Arnold, Engineering new catalytic activities in enzymes. *Nat. Catal.* **3**, 203–213 (2020).

3. M. T-. Gamasa, M. M-. Calvo, J. R. Couceiro, J. L. Mascareñas, Transition metal catalysis in the mitochondria of living cells. *Nat. Comm.* 7, 12538 (2016).

6. F. Schwizer *et al.*, Artificial metalloenzymes: reaction scope and optimization strategies. *Chem. Rev.* **118**, 142–231 (2018).

8. E. V. Vinogradova, C. Zhang, A. M. Spokoyny, B. L. Pentelute, & S. L. Buchwald, Organometallic palladium reagents for cysteine bioconjugation. *Nature* **526**, 687–691 (2015).

10. C .Streu, E. Meggers, Ruthenium-induced allylcarbamate cleavage in living cells. *Angew. Chem. Int. Ed.* **45**, 5645–5648 (2006).

11. S. A. Green *et al*., Regulating transition-metal catalysis through interference by short RNAs. *Angew. Chem. Int. Ed.* **58**, 16400–16404 (2019).

12. A. Ono, *et al*. Specific interactions between silver(I) ions and cytosine-cytosine pairs in DNA duplexes. *Chem. Commun.* **10.1039/b808686a**, 4825–4827 (2008).

13. A. Ono, H. Torigoe, Y, Tanaka, I. Okamoto, Binding of metal ions by pyrimidine base pairs in DNA duplexes. *Chem. Soc. Rev.* **40**, 5855–5866 (2011).

14. H. Mei, I. Röhl, F Seela, Ag^{+}-mediated DNA base pairing: extraordinarily stable pyrrolo-dC–pyrrolo-dC pairs binding two silver ions. *J. Org. Chem.* **78**, 9457–9463 (2013).

16. L. Zhang, E. Meggers, An extremely stable and orthogonal DNA base pair with simplified three-carbon backbone. *J. Am. Chem. Soc.* **127**, 74–75 (2005).

17. J.H. Do, H.N. Kim, Yoon, J., Kim, J. S., H.–J. Kim, A rationally designed fluorescence turn-on probe for the Gold(III) ion. *Org. Lett.* **12**, 932–934, (2010).

18. S. Tyagi, F.R. Kramer, Molecular beacons: probes that fluoresce upon hybridization. *Nat. Biotechnol*. **14**, 303–308 (1996).

19. G. Leone, B. van Gemen, C.D. Schoen, H. van Schijndel, F.R. Kramer, Molecular beacon probes combined with amplification by NASBA enable homogeneous, real-time detection of RNA. *Nucleic Acids Res.* **26**, 2150–2155 (1998).

20. Y. Kim, D. Sohn, W. Tan, Molecular beacons in biomedical detection and clinical Diagnosis. *Int. J. Clin. Exp. Pathol.* **1**, 105–116 (2008).

21. C. Johnston, B. Martin, G. Fichant, P. Polard, J.-P. Claverys, Bacterial transformation: distribution, shared mechanisms and divergent control. *Nat. Rev. Microbiol.* **12**, 181–196 (2014).

22. C. Xi, M. Balberg, S.A. Boppart, L. Raskin, Use of DNA and peptide nucleic acid molecular beacons for detection and quantification of rRNA in solution and in whole cells. *Appl. Environ. Microbiol*. **69**, 5673–5678 (2003).

23. Real-time RT-PCR panel for detection 2019-novel coronavirus. (2020) US Centers for Disease Control and Prevention. https://www.fda.gov/media/134922/download [Accessed 5 July 2020].

24. S. Maddocks, R. Jenkins, "Understanding PCR-Quantitative PCR: Things to Consider" in Understanding PCR: A practical benchtop guide, (Elsevier, 2017), pp 45–52.

25. Y.-W. Tang, J.E. Schmitz, D.H. Persing, C.W. Stratton, Laboratory diagnosis of COVID-19: current issues and challenges. *J. Clin. Microbiol.* **58**, e00512-2 (2020).

28. M. Baer, T. W. Nilsen, C. Costigan, C. Altman, Structure and transcription of a human gene for H1 RNA, the RNA component of human RNase P. *Nucleic Acids Res.* **18**, 97–103 (1990).

29. Diagnostic test for COVID-19 only & supplies. (2020) Centers for Disease Control and Prevention. https://www.cdc.gov/coronavirus/2019-ncov/lab/virus-requests.html [Accessed 6 July 2020].

29. See SI for details-control with incorrect complements